

Characterization of the Red Layer and Pericarp of Processing Tomato using Magnetic Resonance Imaging

Lu Zhang, Diane M. Barrett, and Michael J. McCarthy

Abstract: The characteristics of tomato pericarp are closely associated with peelability, an important quality attribute of processing tomatoes. Different types of tissue exist in the pericarp of tomato. The outermost region of the pericarp, the red layer, is removed with the skin during peeling. This study investigated the morphological features and tissue properties of red layer and pericarp for 3 processing tomato cultivars using magnetic resonance imaging (MRI). The red layer can be visualized in MR images with T_2 weighting, indicating the red layer has different properties compared to the rest of the pericarp region. Tomatoes were imaged with a set of MRI sequences with signal intensity dependent on different water proton properties. Principal component analysis (PCA) of the statistical features revealed clustering of fruit by cultivar. The spatial distribution of cultivars in the PCA score plot followed their rank of peeling performance. MRI demonstrated potential as a nondestructive method to characterize tomato pericarp and evaluate the peelability of processing tomatoes.

Keywords: MRI, PCA, peelability, red layer thickness, tomato

Practical Application: Peelability of tomatoes affects the quality of value-added whole peel and diced tomato products. The properties of the pericarp of tomato are directly related to the peelability of tomatoes. MRI provided a fast and nondestructive method to characterize the properties of tomato pericarp. The result of this work gives insight into the correlation between tomato pericarp characteristics and peelability.

Introduction

The pericarp of tomato fruit is comprised of the skin, exocarp, and the peripheral pericarp (Rock and others 2012). The exocarp includes the cell layers located underneath the skin of the tomato pericarp. The peripheral pericarp is the inner portion of the pericarp under the exocarp. Because the exocarp is more richly colored than the other parts of the pericarp, it is also known as “red layer” (Garcia and Barrett 2006; Rock and others 2012). Vascular bundles, large white-appearing regions in the middle of pericarp, separate the pericarp into regions with different optical properties and cell size (Devaux and others 2008). Montgomery and others (1993) detected distinctive expression patterns of the polygalacturonase gene in the inner and outer parts of the tomato pericarp, and concluded that there is a fundamental difference between the parenchymatous cells within the different regions of the pericarp. In addition, a significant difference in the cell wall noncellulosic neutral sugar composition was found between the cells in the inner and outer pericarp region (Huysamer and others 1997). All previous studies confirmed that the pericarp contains multiple cell types, which have distinctive size, composition, and physiological properties.

Peeling is an essential step in the processing of canned tomatoes. The peelability of tomatoes affects the efficiency of the peeling process and the quality of the final product. During peeling, the skin along with some attached pericarp tissue is removed from the fruit. The collapse and rupture of several layers of cells under the skin are responsible for loosening and removal of the skin (Floros and Chinnan 1988). Since the red layer is located immediate beneath the skin, the red layer is involved in the peeling process of tomatoes. Therefore, the properties of the red layer are considered to be an important factor impacting the peelability of tomatoes (Garcia and others 2006; Barrett and others 2006). The tomato cultivar is another factor that influences the peeling performance. Tomato processors choose cultivars with better peelability based on historical observations of peeling performance (Garcia and others 2006). Several studies have shown that anatomical features and visual texture of the pericarp differs from cultivar to cultivar (Floros and Chinnan 1988; Devaux and others 2008; Mohr 1990; Chu and Thompson 1972). Distinct anatomical features lead to the difference in the peeling performance (Mohr 1990).

Magnetic resonance imaging (MRI) may be used to characterize the relative water proton density and local environment of water protons, and the contrast in the image signal intensities originate from the variation in the water proton properties at a cellular level. The signal intensity in the MR image is dependent on the physiological and morphological properties of a plant cell, such as cell dimension, cell compartment morphology, membrane permeability, macromolecules and water self-diffusion (Van As 2007). The

MS 20120827 Submitted 6/15/2012, Accepted 10/16/2012. Authors Zhang, Barrett and McCarthy are with Dept. of Food Science and Technology; and McCarthy is also with Dept. of Biological and Agricultural Engineering, Univ. of California, Davis One Shields Avenue, Davis, CA 95616, U.S.A. Direct inquiries to author McCarthy (E-mail: mjmcCarthy@ucdavis.edu).

heterogeneous nature of the pericarp tissue provides the basis to characterize the red layer morphologically using MRI. Milczarek and McCarthy (2011) used multiple MR imaging protocols to collect information on the pericarp of processing tomatoes. They demonstrated the feasibility of predicting the peeling outcomes of processing tomatoes using multivariate analysis of the MR images. The reason for the correlation between MR images and tomato peelability was not well understood. To explore the underlying cause of the correlation, it is necessary to investigate the characteristics of the red layer and the pericarp of tomatoes with different peeling performance.

The objectives of this study were to nondestructively examine the red layer in tomato pericarp of three cultivars of processing tomatoes using MR imaging, to characterize the red layer and pericarp tissue based on morphological features and signal intensity of MR images, and to compare the properties of the red layer and pericarp of the tomato cultivars to identify differences in the red layer contributing to the variation in peeling performance.

Materials and Methods

Sample selection

Samples of three California processing tomato cultivars, SUN 6366 (Nunhems US), AB 2 (AB seeds Ltd.), and H 8004 (Heinz Tomato Products), were harvested at the red ripe stage from the same field in Stanislaus county, California, in the 2010 season. Tomatoes were sorted to remove defective samples before MRI measurement.

Physical attribute evaluation

The tomato samples were cut into halves, and a digital caliper was used to measure the thickness of the red layer under the skin at three randomly chosen locations around the fruit circumference. The 3 values were averaged to obtain the red layer thickness of each fruit. Twenty samples from each cultivar were examined to compare the thickness of the red layer.

The peeling performance was determined using three batches of 20 tomatoes from each cultivar. The tomatoes were first exposed to 30 psi steam for 45 s, and then passed over mechanical peel eliminators, consisting of a cord scrubber and pinch rollers (Imdec, Woodland, Calif., U.S.A.). After the peeling process, each sample was visually inspected for the presence of residual peel. The peelability was expressed as the percentage of the tomatoes with peel only attached to the stem scar or with no peel attached (Garcia and Barrett 2006). The average of the peelability of the 3 replicate batches of 20 fruit was reported.

MR image acquisition

Twenty fruit from each cultivar were selected for MR imaging. MRI was performed on a 1T permanent magnet MRI system (Aspect AI, Industrial Area Hevel Modi'in, Shoham, Israel) with

a 60 × 90 mm elliptical RF coil. Tomatoes were placed on a plastic sample holder and manually centered so that the stem-blossom-end axis of fruit aligned with the center of the coil. The key-lock fixture on the sample holder ensured that samples had similar alignment in the magnet. Each image acquired used a longitudinal slice along the stem-blossom-end axis of each tomato. A set of 3 MR images was collected for each sample. A small vial filled with manganese chloride solution was imaged along with the sample to provide a reference for MR signal normalization. A Fast Steady-State Gradient Recall Echo (GRE) sequence with a repetition time (TR) of 3.9 ms, echo time (TE) of 1.9 ms, and flip angle of 25° were used to generate a proton density weighted image. A Spin Echo (SE1) sequence with TR of 200 ms and TE of 60 ms were used to produce a T_1 and T_2 weighted image. T_1 weighted images (SE2) were acquired using another Spin Echo sequence with TR of 100 ms and TE of 6.9 ms. The FOV of MR images is 70 × 70 mm and the thickness of the image slice is 8 mm.

Image analysis

The first step in image analysis is proper image segmentation to separate the red layer from the other parts of the tomato image. Among the 3 images with different contrast origin, the T_1 and T_2 weighted spin echo image (SE1) had enough contrast to differentiate pericarp layers (Figure 1). Thus, segmentation of the pericarp layers was performed on the SE1 image with a customized algorithm in Matlab R2010a (The Mathworks, Natick, Ma., U.S.A.; Supplemental information A1). The stem end and blossom end of the red layer mask was clipped off due to the discontinuity of red layer in the 2 end sections (Figure 2A). The average thickness of red layer was calculated based on the red layer mask and the unit of the thickness was converted from voxel to mm by multiplying the in-plane voxel spatial length (70 mm/128). The signal intensity of the MR images was normalized to the average signal intensity of the reference to eliminate the effect of temperature fluctuations, day-to-day coil tuning variations, and other factors

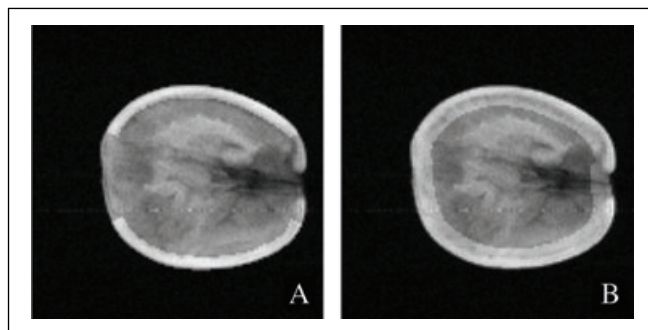


Figure 2—The region of interest (highlighted) for image analysis. (A) red layer mask, (B) pericarp mask.

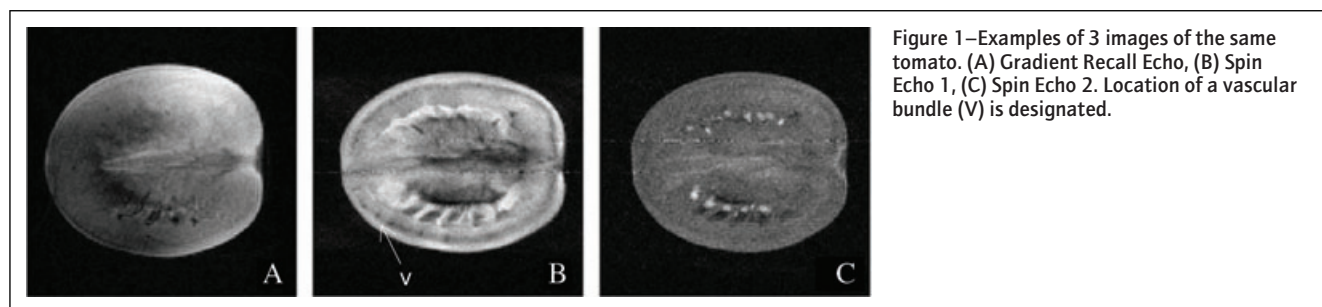


Figure 1—Examples of 3 images of the same tomato. (A) Gradient Recall Echo, (B) Spin Echo 1, (C) Spin Echo 2. Location of a vascular bundle (V) is designated.

on signal intensity. The statistic parameters, mean, variance and coefficient of variance, of the signal intensity in the red layer mask were calculated.

In addition, a pericarp mask was defined arbitrarily as a ring covering the outermost 10 voxels of the tomato object in the image (Figure 2B). The mean, variance, and coefficient of variance, of the signal intensity in the pericarp mask were calculated. Principal component analysis (PCA) was applied to the statistical features of red layer and pericarp calculated from MR images to investigate the underlying pattern or trend in the data. The PCA model was developed using Matlab 2010a (The Mathworks, Natick, Ma., U.S.A.) and PLS_toolbox (Eigenvector research Inc., Wenatchee, Wash. U.S.A.). To validate the model, a 3-fold contiguous blocks cross-validation was performed such that the samples of the same cultivar are all in the calibration subset or all in the validation subset.

Results and Discussion

Morphological features of red layer in MR image

The red layer is recognizable in the spin echo image (SE1) with T_1 and T_2 weighting (Figure 1B). In the MR image, the red layer appeared as a bright spherical layer around the fruit located at the outer region of the pericarp, and it was absent at the stem scar and blossom end as discontinuity of the red layer was observed at these 2 locations in tomatoes. A line of lower signal intensity (darker gray) lay along the red layer in the middle of the pericarp, which served as a clear boundary between outer red layer and the inner pericarp. Vascular bundles appeared as black circles (Figure 1B) lining up with the boundary. The inner layer of the pericarp is slightly darker gray than the red layer in the image as well. The structure of the vascular tissue is distinct from parenchyma cell in the pericarp. According to Devaux and others (2008), vascular bundles appeared as large white spots in the macroscopic image of the pericarp tissue, and the air space occurring between cells in the vascular bundle might be the explanation of its visual white appearance. The occurrence of air spaces will induce magnetic susceptibility variations in the tissue, leading to dephasing of transverse magnetization by the diffusion of water molecules across the interface of inter-cellular air gaps (Hills 2006). In T_2 weighted MR images, lighter gray areas have longer T_2 and darker gray areas have short T_2 . Considering the T_2 weighting in SE1, the low signal intensity in the vascular tissue region in the image originated from the shorter T_2 relaxation time, which is caused by the variation in the magnetic susceptibility. In addition, the internal structure of the tomato is not well resolved in the T_1 weighted SE2 (Figure 1C), except that seeds are visible as small light gray spots. Therefore, the variation in T_2 within the tomato was a major contributor to the contrast in SE1, which enabled the visualization of the red layer in the pericarp. The higher signal intensity in the red layer was due to the longer T_2 relaxation time of red layer, as compared to other tissues in the pericarp. The divergence in the T_2 relaxation time of different cell types in the pericarp supports the previous findings on the difference between the types of cells within the different regions of the pericarp (Montgomery and others 1993; Huysamer and others 1997). The difference in cell size, cell metabolites concentration, or presence of air space may explain the T_2 induced contrast in SE1. For example, the shorter T_2 relaxation time in the inner layer of the pericarp may be a result of higher sugar content or occurrence of intercellular air gaps. Ciampa and others (2010) also observed external spherical layer of pericarp as a light zone in T_2 weighted MR images of cherry tomato.

Table 1—Red layer thickness and characteristic parameters of red layer derived from MR images of 3 tomato cultivars.

		AB 2	H8004	SUN 6366
Red layer thickness (mm)		2.20 ^a	2.21 ^a	2.20 ^a
Red layer thickness (mm)	(MRI)	2.76 ^b	2.85 ^a	2.80 ^b
Mean ($\times 10^2$)	GRE	7.15 ^a	7.26 ^a	6.96 ^a
	SE1	12.21 ^b	11.67 ^b	13.99 ^a
	SE2	2.06 ^b	1.98 ^b	2.29 ^a
Variance ($\times 10^3$)	GRE	144.46 ^a	133.48 ^a	124.49 ^a
	SE1	58.74 ^a	39.95 ^b	58.97 ^a
	SE2	4.31 ^b	3.28 ^b	6.62 ^a
Coefficient of variation	GRE	0.52 ^a	0.50 ^a	0.50 ^a
	SE1	0.20 ^a	0.17 ^b	0.17 ^b
	SE2	0.31 ^{ab}	0.28 ^b	0.33 ^a

Values with the same letters in the same row are not significantly different at $P = .05$. Note: MR, magnetic resonance; GRE, Gradient Recall Echo; SE 1, Spin Echo 1; SE 2, Spin Echo 2.

Thickness of red layer

The red layer thickness was calculated from the red layer mask derived from the SE1 image of each tomato. H 8004 had the thickest red layer among all 3 cultivars, and AB2 had the thinnest red layer (Table 1). Although the difference in the averaged thickness between H 8004 and SUN 6366 was only 0.05 mm, the thickness of the 2 cultivars was statistically significantly different from each other. The MRI derived values for red layer thickness differed from those obtained by physically measuring the red layer with a caliper (Table 1). The caliper measurement was from 3 random locations on the tomato, while the MRI method gave the average of the thickness of the entire red layer in a slice crossing the fruit, excluding the stem scar and blossom end. The value from MR images is more representative of the whole fruit than the caliper measurement. In order to achieve similar performance as the MRI method, the caliper measurement would need to be conducted at a greater number of locations around the whole tomato. The inclusion of the thickness of the skin in the MRI method is another reason for the difference between the 2 methods. Thickness of red layer calculated from MR images was about 0.5 mm larger than the one measured with a caliper.

Quantitative analysis of MR images of red layer

In Nuclear Magnetic Resonance, the excited spins return back to their original state through 2 relaxation processes. T_1 and T_2 relaxation times are used to characterize the 2 relaxation processes. The T_1 and T_2 relaxation times are related to the water content, physical properties of water, and interactions between water and macromolecules (Van As 1992). In an MR image, the signal intensity of each voxel is a function of the proton density, the T_1 and T_2 of protons, thereby reflecting the characteristics such as moisture content, chemical composition, and tissue structure of the imaged object. The weighting of the proton properties in the MR image can be adjusted by manipulating the imaging sequence parameters. The 3 different imaging sequences used in this study measured different water proton properties in the tomatoes.

To quantify the proton properties of water in the sample, statistical features of the region of interest were calculated. The mean, variance, and coefficient of variation of signal intensity of the red layer region in the MR images of the 3 cultivars are shown in Table 1. For each MR image, the reported values are the averages of all the fruit from the same cultivar. The 3 processing tomato cultivars had comparable mean signal intensity in the proton density weighted GRE image, indicating similar water content in the

red layer of AB 2, H 8004, and SUN 6366 cultivars. In the T_1 weighted SE2, the mean signal intensity in the red layer was higher in SUN 6366 than in AB 2 and H 8004, while the values of AB 2 and H 8004 were not significantly different. In T_1 weighted MR images, the signal intensity increases with a decrease in T_1 relaxation time. The high signal intensity in the red layer of SUN 6366 image originated from a relatively short T_1 relaxation time. Due to the relatively long TE used in SE1, T_2 weighting was expected in the image in addition to the T_1 weighting. The T_2 weighting in SE1 did not change the ranking of the average signal intensity in the red layer of the 3 cultivars. SUN 6366 had the highest signal intensity of red layer region of the SE1 image, and therefore the longest T_2 relaxation time. Possible explanation for the lower T_1/T_2 ratio of SUN 6366 is greater water mobility in the red layer of tissue than in other tissues. The difference in water mobility is most likely due to interactions of water with the cellular tissue and their components (Ciampa and others 2010).

As the signal intensity varied within the fruit, the mean of the voxel signal intensities in the ROI was not useful enough in discrimination of the samples. The tissue heterogeneity within the red layer was characterized by extracting additional parameters from the signal intensity, such as the variance and coefficient of variation. Variance is a measure of the variability of the signal intensity in the red layer. The coefficient of variation is a normalized measure of the dispersion of the signal intensity distribution, in which the standard deviation is normalized by the mean. As shown in Table 1, the 3 different tomato cultivars demonstrated a similar pattern of change in the variance and coefficient of variation. The variability of signal intensity in the GRE image was similar for the 3 cultivars. In SE1, AB 2 and SUN 6366 had higher variance than H 8004, and AB 2 had the highest coefficient of variation. The high level of heterogeneity in the red layer tissue was a result of the heterogeneity in cell size, cell metabolite content, or water content, all of which may affect the T_2 value. The red layer tissue of SUN 6366 varied the most in the T_1 weighted SE2. H 8004

Table 2—Characteristic parameters of pericarp derived from MR images of 3 tomato cultivars.

		AB 2	H 8004	SUN 6366
Mean ($\times 10^3$)	GRE	12.61 ^{ab}	12.98 ^a	12.08 ^b
	SE1	14.04 ^a	14.34 ^a	14.16 ^a
	SE2	5.96 ^b	5.92 ^b	6.93 ^a
Variance ($\times 10^3$)	GRE	117.50 ^a	116.44 ^a	109.07 ^b
	SE1	2.41 ^b	2.47 ^b	4.12 ^a
	SE2	2.50 ^b	2.48 ^b	3.97 ^a
Coefficient of variation	GRE	0.61 ^a	0.59 ^b	0.63 ^a
	SE1	0.21 ^a	0.21 ^a	0.21 ^a
	SE2	0.23 ^b	0.23 ^b	0.26 ^a

Values with the same letters in the same row are not significantly different at $P = .05$. Note: MR, magnetic resonance; GRE, Gradient Recall Echo; SE 1, Spin Echo 1; SE 2, Spin Echo 2.

had the most homogeneous red layer tissue with respect to the variability of signal intensity in the SE1 and SE2 images.

Quantitative analysis of MR images of pericarp

The MR image signal intensity demonstrated that the red layer has different proton relaxation properties, when compared to other parts of the pericarp. Quantitative analysis of the signal intensity was performed on the whole pericarp in addition to the red layer (Table 2). H 8004 had the highest average signal intensity of pericarp in the proton density weighted GRE, suggesting a higher water content in the pericarp of the H8004 cultivar than the other 2 cultivars. Unlike the discrepancy in the red layer, the 3 cultivars showed comparable signal intensity in the entire pericarp region in SE1. In SE2, the pericarp region of SUN 6366 demonstrated the highest signal intensity. The stronger intensity in SE2 could be explained by shorter T_1 relaxation time averaged over the whole pericarp of SUN 6366. AB 2 had the highest variance of signal intensity of pericarp in GRE. SUN 6366 showed the biggest variance within the

E: Food Engineering & Physical Properties

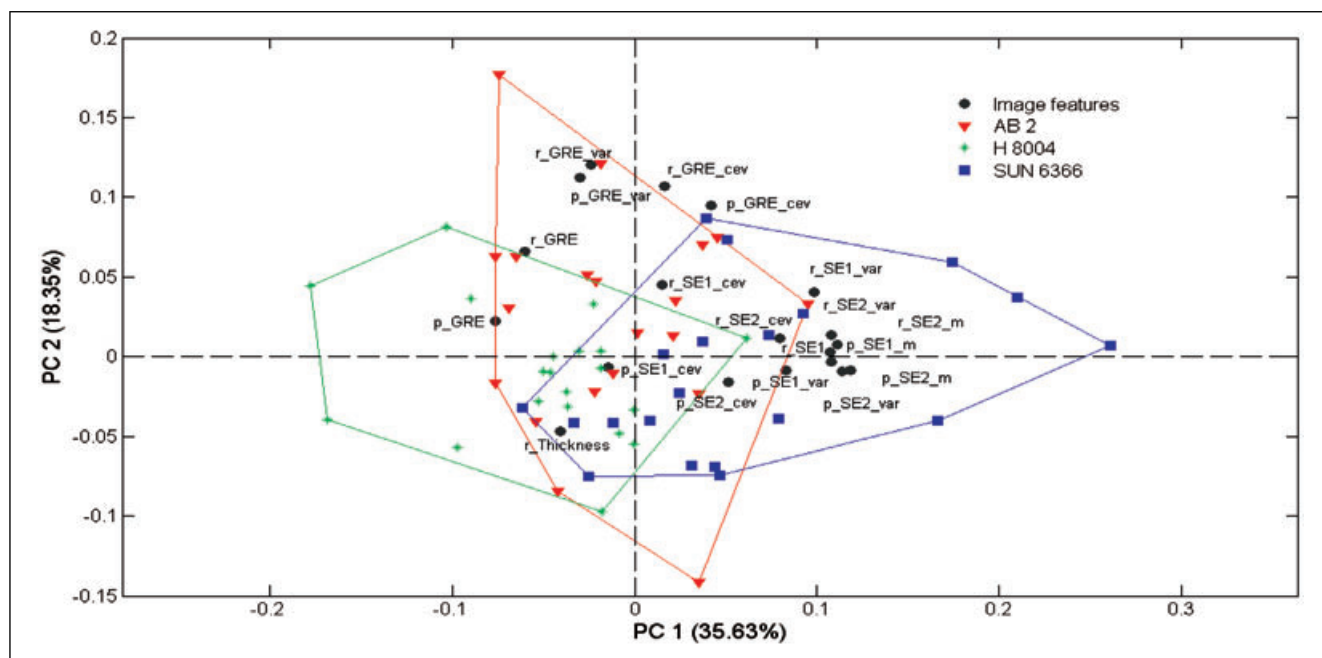


Figure 3—PCA bi-plot (score and loading) of image parameters of red layer and pericarp of tomatoes. Letters refer to: mean, m; var, variance; cev, coefficient of variation; r, red layer; p, pericarp; GRE, Gradient Recall Echo; SE1, Spin Echo 1; SE2, Spin Echo 2.

pericarp region of both SE1 and SE2 image. A similar trend was found in the coefficient of variation in GRE and SE2. Therefore, the pericarp of SUN 6366 was more heterogeneous than AB2 and H 8004.

PCA of the MR images of tomatoes

Some variation existed among the 3 cultivars in terms of the statistical features of red layer and pericarp in MR images, but no clear trend was observed from the features. The multivariate data analysis method PCA was therefore applied to the MR image features to compare the tomato cultivars. The first 2 principal components (PC) accounted for 35.63% and 18.35% of the overall variance. If the variables were highly correlated with each other, the first PC would capture most of the variance within the data. The moderate level of explained variance by the first PC indicated that limited correlation existed among the variables. A bi-plot of the first 2PCs is shown in Figure 3. Although large variation existed within each cultivar, fruit from the same cultivar tended to cluster together. The difference among the 3 cultivars was best described by the first PC. An obvious gradient was observed along the first PC. SUN 6366 samples had the highest scores on PC1, followed by AB2, and H 8004 group had the lowest score on PC1. Each PC is a linear combination of the input variables, and loading defines the contribution of each variable to the PC. As shown in the bi-plot (Figure 3), variables with high loadings on PC1 were mean and variance of signal intensity of pericarp in SE2, mean signal intensity of pericarp in SE1, mean and variance of signal intensity of red layer in SE2, and variance of signal intensity of red layer in SE1. These images features had the greatest contribution to discrimination of the cultivars.

Peeling performance

Among the 3 cultivars, SUN 6366 had the highest peelability of 56.9%, AB2 had a slightly lower peelability 50.9%, and H 8004 had the lowest peelability of 30.4%. The gradient in the PCA bi-plot of tomato samples along PC1 was coincident with the trend in peelability of the tomato cultivars (Figure 3). The overlap between different cultivars indicates the difference between cultivars was not large enough to separate them into well resolved clusters. Similarly, moderate differentiation among the 3 cultivars was shown in the peelability data. Cultivars differ in physical and chemical properties, such as fruit size, shape, color, sugar, and acid content. However, there is biological variation between each individual fruit within the same cultivar, which may diminish the differentiation among cultivars

As noted, mean and variance of signal intensity within red layer and pericarp in SE1 and SE2 were the main variables that differentiated the cultivars. The source of the contrast in SE1 and SE2, T_1 and T_2 relaxation times, are related to the water content, physical properties of water, and interaction between water with macromolecules (Van As 1992). The difference in the peelability of the cultivars is a consequence of the difference in the tissue structure and components. The importance of variance of signal intensity in MR images suggested that the heterogeneity of red layer and pericarp tissue in terms of cellular structure and contents may affect the peelability of tomato fruit. Mohr (1990) identified abrupt cell size gradient in pericarp as a primary factor associated with easy-peel cultivars. Because relaxation time is dependent on the cellular dimension in the tissue, variance of signal intensity within red layer and pericarp may be influenced by the sharp cell size gradient.

Conclusion

In processing tomato varieties, the red layer which is involved in peel removal can be distinguished in an MR image with T_2 weighting. The red layer is expected to have different chemical and physical properties than the inner layer of pericarp at the cellular level. Three common processing cultivars, AB2, H 8004, and SUN 6366, had distinctive red layer and pericarp properties. PCA of the red layer and pericarp features in MR images revealed the gradient of variation among the 3 cultivars. The peelability of tomatoes showed correlation with the red layer and pericarp features in MR images, which gave more insight into the relationship between properties of red layer and pericarp and tomato peelability. MRI can be used to characterize red layer and pericarp of tomato. MRI measurements should prove useful for predicting relative peelability of processing tomato cultivars. Future work is needed to validate the results on a larger collection of cultivars and explore the quantitative relationship between MRI measured pericarp properties and peelability.

References

- Barrett DM, Garcia E, Miyao G. 2006. Defects and peelability of processing tomatoes. *J Food Process Preserv* 30:37–45.
- Chu MC, Thompson AE. 1972. Comparative anatomy of pericarps of four tomato mutant. *J Am Soc Hortic Sci* 97:478–81.
- Ciampa A, Dell'Abate MT, Masetti O, Valentini M, Sequi P. 2010. Seasonal chemical-physical changes of PGI Pachino cherry tomatoes detected by magnetic resonance imaging (MRI). *Food Chem* 122:1253–60.
- Devaux M-F, Bouchet B, Legland D, Guillon F, Lahaye M. 2008. Macro-vision and grey level granulometry for quantification of tomato pericarp structure. *Postharvest Biol Technol* 47:199–209.
- Floros JD, Chinnan MS. 1988. Microstructural changes during steam peeling of fruits and vegetables. *J Food Sci* 53:849–53.
- Garcia E, Barrett DM. 2006. Evaluation of processing tomatoes from two consecutive growing seasons: quality attributes, peelability and yield. *J Food Process Preserv* 30:20–36.
- Garcia E, Watnik MR, Barrett DM. 2006. Can we predict peeling performance of processing tomatoes? *J Food Process Preserv* 30:46–55.
- Hills BP. 2006. NMR relaxation and diffusion studies of horticultural products. In: Webb GA, editor. *Modern Magnetic Resonance*. Netherlands: Springer. p 1721–7.
- Huysamer M, Greve LC, Labavitch JM. 1997. Cell wall metabolism in ripening fruit. VIII. Cell wall composition and synthetic capacity of two regions of the outer pericarp of mature green and red ripe cv. Jackpot tomatoes. *Physiol Plant* 101:314–22.
- Milczarek RR, McCarthy MJ. 2011. Prediction of processing tomato peeling outcomes. *J Food Process Preserv* 35:631–8.
- Mohr WR. 1990. The influence of fruit anatomy on ease of peeling of tomatoes for canning. *Int J Food Sci Tech* 25:449–57.
- Montgomery J, Pollard V, Deikman J, Fischer RL. 1993. Positive and negative regulatory regions control the spatial distribution of polygalacturonase transcription in tomato fruit pericarp. *Plant Cell* 5:1049–62.
- Rock C, Yang W, Goodrich-Schneider R, Feng H. 2012. Conventional and alternative methods for tomato peeling. *Food Eng Rev* 4:1–15.
- Van As H. 1992. NMR in horticulture: in situ plant water balance studies with NMR. *Acta Hortic* 304:103–12.
- Van As H. 2007. Intact plant MRI for the study of cell water relations, membrane permeability, cell-to-cell and long distance water transport. *J Exp Bot* 58:743–56.

Supporting Information

Additional Supporting Information may be found in the online version of this article at the publisher's web site:

A1. Image segmentation procedure

The image segmentation procedure is shown in Figure A1. A 5×5 Gaussian low pass filter was implemented on the SE1 image (Figure A2a) to smooth the MR image (Figure A2b). An additive image of the second derivatives of the filtered image in the x and y direction was obtained to identify the boundary between the red layer and the inner pericarp layer (Figure A2c). Image erosion (disk, $r = 2$) was applied to the derivative image to fill in the gap between the inner and outer perimeter of the red layer (Figure A2d). A binary mask of the whole tomato was created using Otsu's auto thresholding method (Figure A2e). The eroded image was multiplied by the binary mask to remove background voxels

(Figure A2f). A rough mask of red layer is generated by image thresholding (Figure A2g). However, some small foreign objects were attached to the mask or scattered in the image. Scattered small objects were removed from the mask by “bwareaopen.m” (Figure A2h). Because the red layer mask was an elliptical ring with thickness of about 5 voxels, image operations “imopen.m” and “imclose.m” would change the shape of the mask dramatically. In order to remove the small objects attached to the mask and small gaps within the red layer mask, further morphology operations including “imclose.m”, “imfill.m”, and “imopen.m” were implemented on the complement of the rough red layer mask (Figure A2i). A smooth red layer mask was obtained by calculating the complement of the polished complement of the rough red layer mask. Then, the stem end and blossom end of the red

layer mask were clipped off due to the discontinuity of red layer in the two end sections (Figure A2j). The Euclidean distances of all voxels on the inner perimeter of the red layer mask to the outermost edge of the mask were average to calculate the red layer thickness.

Figure A1. Schematic flow chart of image segmentation procedure.

Figure A2. Results of each image segmentation step. (a) original Spin Echo 1 image, (b) Gaussian low pass filter smoothed image, (c) second derivative of the smoothed image, (d) eroded image, (e) binary mask of the tomato, (f) background removed from the image, (g) rough red layer mask, (h) small objects removed from the mask, (i) complement of the rough red layer mask, (j) red layer mask, (k) the red layer mask overlaid on the Spin Echo 1 image.